JOURNAL OF APPLIED ELECTROCHEMISTRY 22 (1992) 1039–1048

Development of long-lived high-performance zinc–calcium/nickel oxide cells

R. JAIN*, T. C. ADLER, F. R. McLARNON‡, E. J. CAIRNS

Energy & Environment Division, Lawrence Berkeley Laboratory and Department of Chemical Engineering, University of California, Berkeley, CA 94720, USA

Received 3 February 1992; revised 8 April 1992

The addition of $Ca(OH)_2$ to the zinc electrode of Zn/KOH/NiOOH cells was investigated in order to determine its effect on the rate of zinc active material redistribution (shape change) and cell cycle-life performance. Cells of equal mass and capacity, and therefore the same specific energy, containing 0, 10, 25, and 40 mol % $Ca(OH)_2$ in their zinc electrodes were constructed and tested. The $Ca(OH)_2$ and $Zn(OH)_4^{2-}$-supersaturated KOH solution formed a calcium–zincate complex during the discharge half-cycle. The solubility of this complex is less than that of ZnO, and the lower zinc species solubility leads to a slower rate of Zn redistribution, thereby extending the cell cycle life. The best cells tested were those with 25%-$Ca(OH)_2$ electrodes, which lost capacity at a rate of 0.13%/cycle, compared to 0.47%/cycle in calcium-free control cells constructed in the same manner. Also, zinc active material utilization in the calcium-containing electrodes showed a dramatic improvement, compared to the calcium-free zinc electrodes.

1. Introduction

The Zn/NiOOH couple has a sufficiently high theoretical specific energy ($326\,Wh\,kg^{-1}$) that it can be expected to deliver about $75\,Wh\,kg^{-1}$ in a well-designed monopolar rechargeable battery. High specific energy, excellent power performance ($> 130\,W\,kg^{-1}$), good performance even during very cold ambient conditions ($-20\,°C$), inexpensive materials, and low-toxicity materials make the Zn/NiOOH battery a good choice for portable power applications [1]. Significant research and development of this battery has been carried out, but two important problems remain. One problem is that the cost of the battery is still fairly high due to the cost of the NiOOH electrode. The other important problem is the limited lifetime of this battery; it rarely completes more than 200 full-capacity (100% DOD) cycles before failing. Failure is typically associated with two phenomena: (i) zinc dendrite initiation and propagation, leading to cell shorting, and (ii) zinc material redistribution (shape change), leading to gradual capacity loss.

Zinc active material can migrate across the face of the electrode (in a direction parallel to the face of the electrode), into or out of the pores of the electrode (perpendicular to the face of the electrode), and away from the electrode to the NiOOH electrode. These migration processes result in regions of the electrode with dense and nodular zinc, and regions which have very little or no zinc. The results of these processes include (i) reduced capacity of the NiOOH electrode, because of a lack of zinc active material in close proximity to portions of the NiOOH electrode, (ii) the zinc electrode may become the capacity-limiting electrode, even if there was a large excess stoichiometric quantity of zinc early in cell life, and (iii) dense areas of zinc can grow large enough to puncture the separator and short the cell.

The fundamental cause of zinc electrode shape change is not known with certainty, however various mechanisms have been proposed to offer an explanation [1]. These mechanisms include (i) electrolyte flow caused by osmotic pressure gradients in cells with ion-exchange separators, (ii) electrolyte concentration gradients caused by the difference between the current density distribution during charge and that during discharge, (iii) natural convection of the electrolyte caused by density gradients, (iv) autocatalytic zinc dissolution from the periphery of the zinc electrode, (v) lower charge efficiency for the zinc deposition reaction at the electrode periphery caused by non-uniform OH^--ion concentration, and (vi) oxidation of zinc to soluble ZnO by oxygen that has migrated from the NiOOH electrode (where it is evolved during charge) to the periphery of the zinc electrode. Various experimental methods have been applied to characterize observed shape change processes in rechargeable alkaline zinc cells [1], including post-test measurements of zinc material distributions, direct sampling of the electrolyte concentration during cell cycling experiments, radiotracer studies of species distributions, and the use of microreference electrodes to measure electrolyte concentrations in cycling cells. Most of these studies indicated that electrolyte movement is an important factor in determining the rate

* Present address: 254-E College Avenue, Palo Alto, CA 94306, USA.
‡ Author to whom all correspondence should be sent.

0021-891X

and extent of zinc material redistribution, which lends qualitative support to mechanisms (i) and (iii) above. However, none of the models can fully account for the shape-change phenomenon, particularly the observation that zinc can migrate either toward *or* away from the centre of the electrode [1]. However all of the models suggest that if the amount of zinc dissolved in the electrolyte is decreased, the rate of zinc redistribution will decrease. It is the high solubility of $Zn(OH)_4^{2-}$ ion (zincate) in alkaline solutions, and the propensity for the formation of zincate-supersaturated electrolyte solutions during discharge, that is strongly associated with the shape-change process.

Among the methods that can be used to reduce the solubility of zincate ion in alkaline electrolytes, the addition of $Ca(OH)_2$ to the Zn–ZnO electrode has long been recognized as useful [2–4], and is covered in the patent literature [5–7]. The intent is to form a relatively insoluble complex with ZnO, thereby maintaining much of the Zn in a solid form, but allow the interconversion of Zn to ZnO at sufficiently high rates to permit the cell to be charged and discharged. Calcium hydroxide is insoluble in alkaline solutions, and would therefore retain a uniform distribution as the cell is cycled. Furthermore $Ca(OH)_2$ is non-toxic and inexpensive. Kawamura and Maki's experiments indicated that other alkaline-earth metal hydroxides were not as effective as $Ca(OH)_2$ in complexing with zinc species [8].

2. The calcium–zinc complex

Calcium–zincate complexes have been studied not only because of their potential use in secondary alkaline zinc electrodes, but also because they are important in other technologies. For example, calcium zincate forms as Zn corrodes in concrete [9], it is used to impart higher strength to concrete and mortar [10], and it has been used as a component of wood adhesives [11]. Other calcium–zincate complexes have found uses as polymerization catalysts, phosphors, dielectrics, and industrial glasses.

There have been several investigations of the stoichiometry of calcium zincate, using atomic-absorption analysis [8], thermal-gravimetric analysis [12], powder X-ray diffraction [8, 9, 12–15], and other techniques [4, 16]. Reported stoichiometric ratios of $Ca(OH)_2$/$Zn(OH)_2$ in calcium zincate include 1/1 [4, 15], 2/3 [8] and 1/2 [9, 10, 12–14, 16]. The 1/2 Ca/Zn compound is reported to contain two waters of hydration [9, 10, 12, 16]. Calcium zincate exhibits a distinctive powder X-ray diffraction pattern [8, 12–14], and its density [12–14] and crystallographic parameters [9, 15] have been reported. Both hexagonal [15] and tetragonal [8, 12, 15, 17] crystal habits have been observed.

3. Zinc–calcium electrodes

An important issue in the design of ZnCa electrodes for use in secondary Zn/NiOOH cells is the selection of the stoichiometric ratio of $Ca(OH)_2$ to ZnO used in the electrode mix. The above discussion of the stoichiometry of the calcium–zincate complex suggests that a Ca/Zn molar ratio of at least 1/2 would provide sufficient calcium to complex the available zinc, and thereby minimize the amount of soluble zinc that is available to migrate throughout the cell. However, the $Ca(OH)_2$ adds unwanted inert mass to the cell and thereby decreases the cell specific energy, provided that a high stoichiometric Zn/Ni ratio is maintained (a Zn/Ni ratio of about 3/1 is typical for Zn/NiOOH cells). This has been the case in prior studies of ZnCa/NiOOH cells, wherein the molar ratio of Ca/Zn was varied from 0/1 to 1/1 [17–20], but a large Zn/Ni ratio was maintained. One study found that a Ca/Zn molar ratio of 0.58/1, which is near to the probable stoichiometric ratio of calcium zincate, is best [19]. Investigations of large-size battery packs have confirmed the decrease in specific energy that accompanies calcium additions to Zn/NiOOH cells when a high Zn/Ni stoichiometric ratio is maintained [21, 22]. The present work seeks to evaluate the cycle-life performance of ZnCa/NiOOH cells in which the $Ca(OH)_2$ additions are balanced by reducing the stoichiometric Zn/Ni ratio, in order to preserve the mass characteristic of a 'baseline' Zn/NiOOH cell. So long as the zinc active material can be utilized in such a cell, the good specific energy characteristics of the Zn/NiOOH cell will be maintained.

The rate at which ZnCa/NiOOH cells can be charged and discharged will depend upon the rate of decomposition and formation, respectively, of the calcium-zincate complex. Kinetic studies of the zinc–calcium complex have shown that the decomposition rate of the complex is relatively fast, however the formation rate can be slow [23, 24]. The effects of KOH concentration on the zinc–calcium complex formation/decomposition kinetics, and corresponding ZnCa/NiOOH cell performance, have been investigated [25, 26]. The formation rate of the complex is clearly favoured by the use of low concentrations of KOH, and minimum rates of zinc-electrode shape change are seen at 10 wt % KOH. However, the cell performance is compromised at such low electrolyte concentrations, particularly at lower temperatures.

Sato *et al.* prepared a sealed ZnCa/NiOOH cell that employed a novel separator and reverse-pulse charging, and attained > 500 cycles on a C-size cell [27]. Adler *et al.* obtained good cycle-life performance by pulse-charging a cell that combined ZnCa electrodes with KF–KOH electrolyte (which suppressed the solubility of zinc species by a factor of four below that in 31 wt % KOH electrolyte), however the results were not repeatable [28]. MacArthur analysed the performance and costs of 20 Ah ZnCa/NiOOH cells, and his results illustrate the difficulty in simultaneously meeting performance, durability and cost requirements [29]. McBreen has conducted fundamental electrochemical investigations of the ZnCa electrode [30].

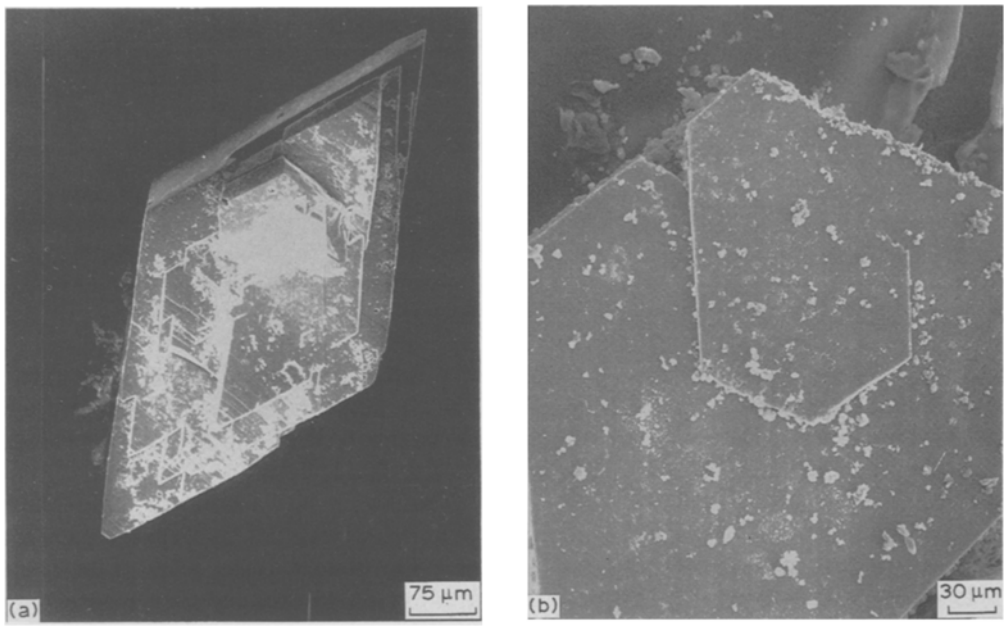

Fig. 1. Stacking dislocations in calcium zincate crystals highlighting two crystal habits. (a) Tetragonal-shape dislocation, and (b) hexagonal-shape dislocation.

4. Formation and analysis of calcium zincate

Beaker experiments were carried out to assess the rate of reaction between $Ca(OH)_2$ and zincate-saturated 31 wt % KOH. Small quantities of tetragonal and hexagonal crystals were formed, and the observed rates of formation confirmed prior observations that the reaction to form calcium zincate in 31 wt % KOH is slow. To evaluate the possible effects of zincate supersaturation on the rate of calcium zincate formation, 10 to 20 ml of deionized water was added to a beaker containing 100 ml of 31% KOH and a few grams each of ZnO and $Ca(OH)_2$. Within 30 min, small crystals could be seen with the unaided eye, and within a few hours large crystals, ~0.5 mm long, were observed. These crystals, shown in Fig. 1(a), were of a tetragonal form and exhibited the same powder X-ray pattern as that reported for the hexagonal crystal [8, 13, 14]. A hexagonal-shape crystal is shown in Fig. 1(b). The as-formed calcium zincate crystals are fairly stable. When calcium zincate crystals were added to pure 46% KOH (which contained no ZnO or $Ca(OH)_2$), some remained undissolved after 3 h. It is interesting to note that even though the hexagonal and tetragonal crystals are indeed different crystal structures, as illustrated by the crystalline dislocations displayed in Fig. 1(a) and (b), they exhibit the same powder X-ray diffraction pattern [31]. Unfortunately, the crystals were too small for X-ray crystallography to be carried out. Chemical analyses using atomic absorption and X-ray fluorescence demonstrated that the Zn/Ca ratios were 2.0 for the tetragonal crystal and 2.1 for the hexagonal crystal, respectively. A very small amount of the hexagonal crystal was produced so the analysis of it is less accurate. The Zn/Ca ratio of 2/1 agrees with the formulae given in a powder X-ray diffraction handbook [14] and that reported by others [9, 10, 12, 13, 16]. In addition, the density of the tetragonal crystal was experimentally determined and found to be 2.63 g cm^{-3}, which may be compared to the value of 2.62 g cm^{-3} by Liebau and Amel-Zadch [13], 2.60 g cm^{-3} reported by Schwick [14], and 2.59 g cm^{-3} reported by Sharma [12]. A hydrogen-liberation analysis of the calcium zincate was performed, and it indicated 3.26% of hydrogen. The amount of hydrogen agrees with the formula unit $Ca(OH)_2 \cdot 2[Zn(OH)_2] \cdot 2H_2O$, however waters of hydration were not determined.

The hexagonal crystal structure was observed only when the complex was allowed to form very slowly (over a period of days) in a saturated solution, whereas the tetragonal structure was observed when the complex formed quickly due to supersaturation. It is expected that when used in Zn/NiOOH cells, the calcium zincate will be observed in the tetragonal structure.

5. Experimental procedures

In order to determine the effect of $Ca(OH)_2$ additions to the zinc electrode on the cycle-life performance of a Zn/NiOOH cell, experimental cells were constructed, cycled for extended periods, and then examined in detail. Table 1 lists the quantities of materials used to prepare the negative electrode of the cells that were tested. The four cell types are identified by the relative amounts of ZnO and $Ca(OH)_2$, expressed as the mol % of $Ca(OH)_2$ in the ZnO and $Ca(OH)_2$ [i.e. ignoring the PbO and polytetrafluoroethylene (PTFE) content]. The 0%-Ca cells represent baseline Zn/NiOOH cells, and the calcium content of the other cells was varied in order to determine the amount of calcium that might be optimal for cells of this type. Note that calcium additions were balanced by reducing the amount of ZnO contained in the cell.

A cell consisted of a zinc electrode held between two

Table 1. Composition of negative electrodes

Cell type /mol% Ca*	*Replicates*	*$Ca(OH)_2$* /g	*ZnO* /g	*PbO* /g	*PTFE* /g	*Excess ZnO*	
						/g	/%
0% Ca	2	0	6.0	0.13 (2%)	0.26 (4%)	4.0	200
10% Ca	4	0.55	5.45	0.13	0.26	3.45	175
25% Ca	3	1.40	4.60	0.13	0.32 (5%)	2.60	130
40% Ca	3	2.27	3.74	0.13	0.38 (6%)	1.74	85

* Expressed as the moles of $Ca(OH)_2$ divided by the moles of ZnO plus $Ca(OH)_2$ times 100.

NiOOH electrodes, and the capacity of each NiOOH electrode was one-half that of the 1.32 Ah cell design capacity. Each electrode was 70 mm wide by 62 mm high. In addition to the ZnO and $Ca(OH)_2$, the zinc electrode also contained small amounts of PbO (to suppress hydrogen evolution) and 4–6% PTFE added as a binder. Because the density of $Ca(OH)_2$ is 2.24 g cm^{-3}, which may be compared to 5.61 g cm^{-3} for ZnO, the 25%-Ca and 40%-Ca electrodes occupied a significantly greater volume than electrodes with smaller calcium content, and therefore required more binder. The PTFE used was TFE-30 (E.I. DuPont De Nemours and Co.), which is a dispersion of PTFE with 5.5% Triton X-100 (added as a wetting agent) in water.

The current collector for the zinc electrode was an expanded-metal copper mesh (4-Cu-7, Die Mesh Corporation of Mount Vernon, New York) electroplated with 0.3 g of lead using an aqueous lead fluoroborate solution. The lead plate was roughly 4 μm thick. The procedure for preparing the zinc electrodes was similar to that reported elsewhere [28, 32], and details are provided in [31]. The final porosity of the zinc electrodes was about 75% for the 0%-Ca and 10%-Ca electrodes, and about 70% for the 25%-Ca and 40%-Ca electrodes (porosities based on the as-prepared electrodes). The sintered NiOOH electrodes were purchased from Eagle Picher Co. as sheets and cut to the required sizes. The loading of the NiOOH electrodes was 0.055 g $Ni(OH)_2$ cm^{-2}.

All zinc electrodes were wrapped with three layers of Celgard 3401 separator, which is a microporous polypropylene sheet (0.02 μm effective pore size) manufactured by Celanese Fibers Corporation. Each layer was individually heat sealed as close as possible to the edges of the electrode. The separator seal at the top of the electrode was < 3 mm above the electrode edge in the 40%-Ca cells, one of the 0%-Ca cells, two of the 10%-Ca cells, and one of the 25%-Ca cells. For all the other electrodes the seal was roughly 0.6–1.3 cm above the top of the electrode edge. The proximity of the seal to the electrode is a very important parameter, as discussed below. Each NiOOH electrode was wrapped with a layer of Pellon 2502K4 non-woven nylon wick material (Pellon Corporation). The cell was assembled so that the zinc electrode initially was under a pressure of 28 kN m^{-2}, fitted with a Hg/HgO reference electrode, and filled with 31 wt % KOH–1 wt % LiOH electrolyte which was saturated with ZnO (chemicals J. T. Baker reagent grade, and water 15 MΩ or better). The electrolyte level was ~ 0.6 cm above the top edge of the electrodes, and all cells were operated in a vented, flooded-electrolyte mode.

The cells were cycled using a computer-controlled system described in [33]. Cells were initially subjected to 3–4 formation cycles, wherein the cell was charged at a low (20 h) rate and then discharged at the 2.5 h rate until the potential of the zinc electrode reached − 1.0 V (against Hg/HgO). The formation cycle discharge was continued at progressively smaller currents (down to 0.01 A), while maintaining the zinc electrode potential below − 1.0 V, to essentially deplete the cell capacity. The cells were then subjected to regular cycling, performed at a 5 h charge rate of 0.263 A and a 2.5 h discharge rate of 0.526 A. For the 40%-Ca cells a high overpotential at the zinc electrode during charge caused the cell to short after only a few cycles, and the 25%-Ca electrodes also exhibited above-average and erratic overpotentials at the 0.263 A charging rate, so the charge rate was decreased by 24% to 0.200 A. The cells were charged at constant current until the proper number of Ah were passed (1–5% overcharge was used), or until an upper voltage limit was reached, followed by a 10 min open-circuit stand. This was followed by a constant-current discharge until either the cell voltage or the zinc electrode potential exceeded specified values (1.0 V and − 1.0 V against Hg/HgO, respectively), or the 1.32 Ah the design capacity was reached, followed by another 10-min open-circuit stand before beginning the next charge. When the zinc electrode potential increased near the end of charge, signalling a depletion of the available ZnO reserve, a reformation cycle (full discharge at a low rate, followed by recharge) was performed. Cycling continued until either the cell shorted, the cell capacity dropped and remained below 70% of its original value, or 150 cycles were reached.

After cycling was completed, the cells were weighed, disassembled, and chemically analysed. X-ray photographs (60 keV energy, 100 mAs exposure) of the zinc electrode were recorded, and portions of both the Zn and NiOOH electrodes were removed for SEM analysis (AMR Model 1000, KEVEX attachment) and powder X-ray diffraction studies (Siemens Kristalloflex Diffraktometer). Atomic absorption spectrometry (AAS) was used for all metal analyses, which should result in ~ 2% error. The amount of hydrogen

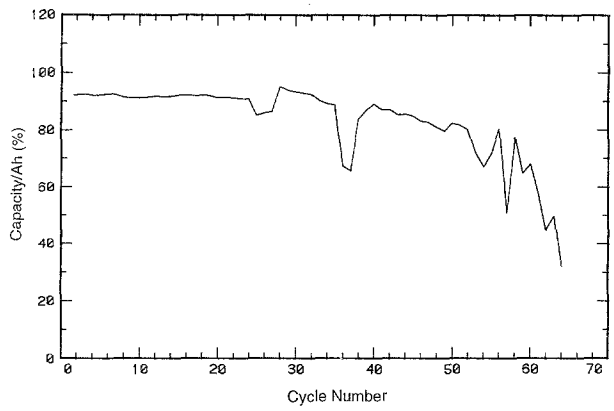

Fig. 2. Capacity against cycle number for Cell 0%-Ca (No. 2). The large spikes in the curve indicate reformation cycles (see text).

was measured by combustion analysis. X-ray fluorescence analysis was attempted, but showed inconsistent results.

6. Results and discussion

The capacity of a 'baseline' 0%-Ca cell versus cycle number is shown in Fig. 2, and voltage–time curves for this cell are shown in Fig. 3. To compare the performance of the various cells, special note will be made of the total charge the cell received vs the grams of excess ZnO present. Because excess ZnO is required to replace the zinc lost via shape change, an increase in the charge passed per unit mass of excess ZnO implies that the rate of zinc shape change had decreased. The excess ZnO for this baseline cell was 4 g (based on the design capacity of 1.32 Ah; slightly more than 4 g, based on the actual initial capacity), and ~ 176 Ah of charge was passed, therefore the electrode received $176/4 = 44\,\mathrm{Ah\,g^{-1}}$ of excess ZnO. Table 2 lists characteristic performance values for this cell and the other cells that were cycled. Note that the separators around this electrode were sealed far from the top edge of the electrode, whereas its replicate had separators that were sealed close to the top edge of the electrode.

Two of the cells with zinc electrodes containing

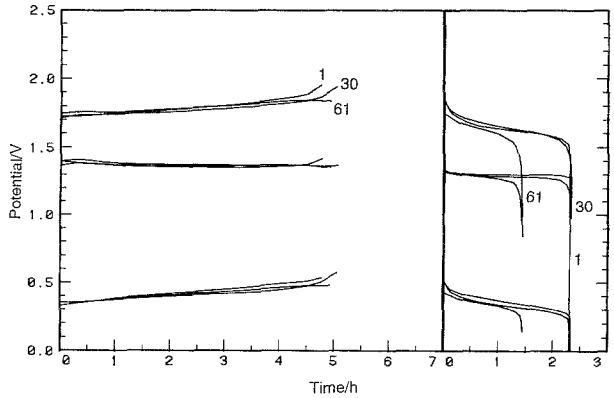

Fig. 3. Voltage against state of charge curves for representative cycles of Cell 0%-Ca (No. 2). The curves represent the cell potential, the negative of the zinc electrode potential (against Hg/HgO), and the NiOOH electrode potential (against Hg/HgO), respectively, from top to bottom. The left-hand portion of the plot shows cell charge, and the right-hand portion shows cell discharge. The numerical annotations indicate the cycle number.

10 mol % Ca had high separator seals, and the NiOOH electrodes used in these cells were not well behaved. However, the performances of these cells were similar to the comparable baseline cell 0%-Ca (No. 2). The other cells in this group had low separator seals and well-behaved NiOOH electrodes. Cell 10%-Ca No. 4 tended to be Zn-electrode limiting during discharge and eventually shorted.

The cells with 25 mol % Ca exhibited the best cycle-life performance. Cells No. 1 and No. 2 in this group contained poorly behaved NiOOH electrodes and were constructed with a high separator seal. The charge current was reduced from 0.26 A to 0.20 A in these cells in order to avoid erratic overpotentials on the NiOOH electrodes. Figure 4 shows the capacity against cycle number for Cell 25%-Ca No. 1, and Fig. 5 shows typical voltage vs time curves for the same cell.

The 40%-Ca cells shorted within the first few cycles, apparently because they could not accept the charge current of 0.263 A. Also, when the negative electrode expanded during the discharge cycle (the specific volume of calcium zincate is larger than that of ZnO and $Ca(OH)_2$ combined), the separators ripped along their seams, which permitted greater rates of dendrite propagation. The separator seals on the 25%-Ca and 10%-Ca electrodes were less-tightly-fitting than those on the 40%-Ca electrodes, in an attempt to mitigate this problem. However, zinc electrode shape change is exacerbated by loosely-fitting separators, and a design trade-off is indicated to arrive at an optimum separator sealing and assembly procedure.

It is clear from the performance data presented in Table 2 that the high separator seal compromises the cycle-life performance of the cells, and that 25 mol % calcium electrodes offer the best performance. The average capacity loss, expressed as percent per cycle, is listed for the cells that did not short. Cell 25%-Ca No. 2 showed no capacity loss up to cycle 97, when a short developed. Also, the 25%-Ca cells exhibited a much-better utilization of the excess ZnO present, implying a reduced rate of shape change. The cell capacity-loss rates presented here are comparable to the best values reported in the literature [19].

X-ray and regular photographs of the zinc electrode from Cells 0%-Ca (No. 2) and 25%-Ca (No. 1) are shown in Figs. 6 and 7, respectively. The calcium-containing electrodes generally showed a modest amount of shape change, compared to the calcium-free electrodes. There was general migration towards the edges of the electrode in most cells, however in one cell (10%-Ca No. 3) there was migration toward the centre of the electrode. Also, some of the electrodes showed zinc material redistribution toward the tab side. The X-ray images of all of the calcium-containing electrodes showed a fairly uniform background material (which is not readily visible in the reproduction shown in Fig. 7(a)), along with 'islands' of denser material. This is in marked contrast to the calcium-free electrodes, wherein there were areas totally devoid of active material (Fig. 6). The electrodes with the high

Table 2. Cell performance

Cell (No.)	*Cycles completed*	*Capacity loss /%/cycle*	*Reason for termination*	*Seal type*	*Excess ZnO* /Ah g^{-1}*
0%-Ca (1)	150	0.06	150 cycles	Low	42
0%-Ca (2)	64	0.47	Low capacity	High	19
10%-Ca (1)	64	0.51	Low capacity	High	21
10%-Ca (2)	71	0.40	Low capacity	High	23
10%-Ca (3)	103	0.12	–	Low	39
10%-Ca (4)	84	0.37	Shorted	Low	29
25%-Ca (1)	150	0.04	150 cycles	High	75
25%-Ca (2)	106	0.22	Shorted	High	52
25%-Ca (3)	150	0.09	150 cycles	Low	67
40%-Ca (1)	2	–	Shorted	Low	–
40%-Ca (2)	2	–	Shorted	Low	–
40%-Ca (3)	2	–	Shorted	Low	–

* Based on the initial cell capacity.

seal show an enhanced rate of zinc redistribution, and in the calcium-free electrode with a high seal, zinc tended to accumulate above the top edge of the electrode (Fig. 6(a)).

SEM/EDAX was used to determine chemical variations over microscopic areas of the electrodes, including the chemical identity of individual crystals or spots of powder. Additional analyses were carried out using X-ray powder diffraction, in order to determine the chemical state of the elements that were present. Figure 8 is a sketch showing the distinct regions of a typical cycled zinc electrode.

The electrodes with 10 and 25% $Ca(OH)_2$ showed a very interesting morphology. Area 1 was mostly ZnO powder, which suggests that there was little migration of calcium compounds from the main body of the electrode. Area 2 contained mostly crystalline calcium zincate with varying amounts of zinc packed around the crystals, as illustrated by the photographs in Fig. 9. In general, there tends to be a greater amount of zinc material near the electrode edges, compared to the central regions. All of the calcium was present as calcium zincate (all cells except Cell 10%-Ca No. 3 were disassembled in the discharged state). The 25%-Ca electrodes contained very little of area 2, compared to the 10%-Ca electrodes. Area 3 was almost all crystalline calcium zincate, as seen in Fig. 10. In the 25%-Ca electrodes, area 3 constituted the majority of the surface. The morphology seen in Fig. 10(c) is most typical of this region. Most of the crystals were tetragonal, with very little hexagonal calcium zincate found. Area 4 (the 'islands') consisted of a calcium zincate layer covered by a layer of ZnO, and area 5 consisted of dense Zn/ZnO powder. There was much more growth of area 5 at the edges of the 10%-Ca electrodes than in the 25%-Ca cells, which may be a consequence of the greater availability of excess ZnO in the 10%-Ca electrodes. Chemical analyses of samples harvested from various locations across the face of 25%-Ca (No. 1) electrode showed that the amount of calcium varied by less than 8%, and the measured ratio of two zinc to one calcium was the value expected for calcium zincate.

Other areas of the cell investigated included the separator, the nylon wicks, and NiOOH electrodes. Both the separator and the nylon wicks had large crystals of the complex adhering to them. The migration of calcium was most likely caused by electrolyte convection, with the calcium-containing particles escaping through the top unsealed tab area of the electrode. The morphologies of the 0%-Ca and 40%-Ca electrodes were also examined, however the results are of lesser interest because of the poor cycle-life performance exhibited by the cells. The results of these investigations are reported elsewhere [31].

Cell 10%-Ca (No. 3) was disassembled in the charged state to assess possible differences between

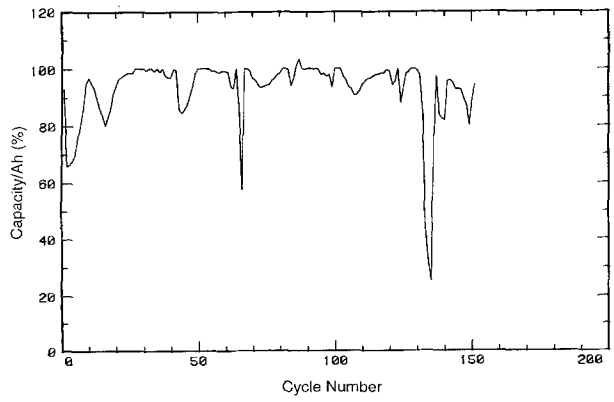

Fig. 4. Capacity against cycle number for Cell 25%-Ca (No. 1).

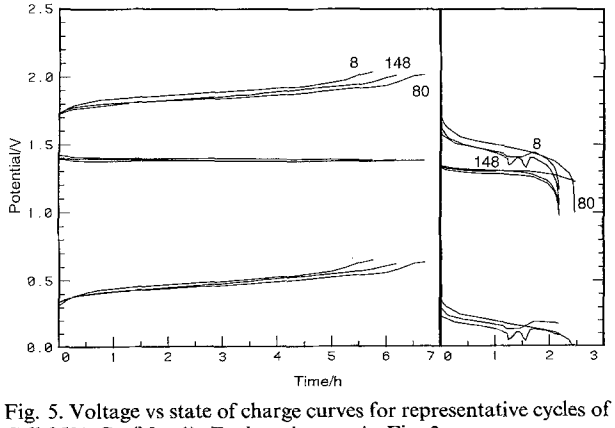

Fig. 5. Voltage vs state of charge curves for representative cycles of Cell 25%-Ca (No. 1). Designations as in Fig. 3.

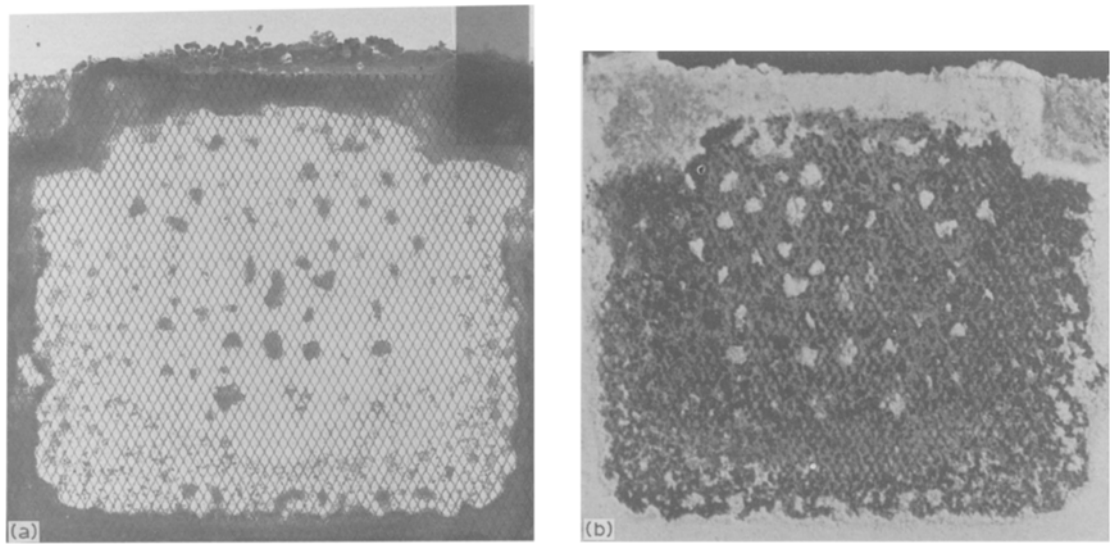

Fig. 6. Zinc electrode from Cell 0%-ca (No. 2) after testing was terminated at cycle 64. (a) X-ray photograph, and (b) normal photograph.

the electrode morphologies in the charged against the discharged state. This electrode showed a considerable amount of uncomplexed $Ca(OH)_2$, and near the electrode edges very little zinc material was found. The isolation of the $Ca(OH)_2$ from the zinc at the edges of this cell implies that considerable zinc migration must occur during single charge and discharge half-cycles (because calcium is present only as calcium zincate in discharged cells). The centre region of the electrode, however, is quite different. The top layer of this material was all metallic zinc, and close to the current collector there was a significant amount of calcium zincate and metallic zinc, and smaller amounts of $Ca(OH)_2$ and some ZnO.

A full material balance was performed on Cell 25%-Ca (No. 1) to assess the rate of migration of zinc to the NiOOH electrode, and to determine if any calcium had migrated to the other areas of the cell or into the electrolyte. The total measured amount of zinc and calcium in the virgin and cycled cells agreed to within 2%, which is well within experimental error. About 65% of the zinc initially present in the negative electrode remained after cycling, whereas $> 85\%$ of the calcium remained. More than 95% of the zinc that left the negative electrode became incorporated into the NiOOH electrodes. The LiOH concentration in the cycled electrolyte was approximately one-third of the original value. A summary of the amount of zinc found in the NiOOH electrodes as a function of the number of cycles is given in Table 3 and plotted in Fig. 11. First, it can be seen that amount of $Ca(OH)_2$ present in the negative electrode had little effect on the zinc migration to the NiOOH electrodes. Second, it is apparent that the migration occurs rapidly in early cycles and then proceeds slowly.

7. Summary and conclusions

Calcium hydroxide was found to react with zincate solutions, forming a crystalline calcium zincate compound. The formation of this compound was fairly rapid in zincate-supersaturated 31% KOH solution, whereas in undersaturated 31% KOH solutions the reaction is very slow. The addition of $Ca(OH)_2$ to the

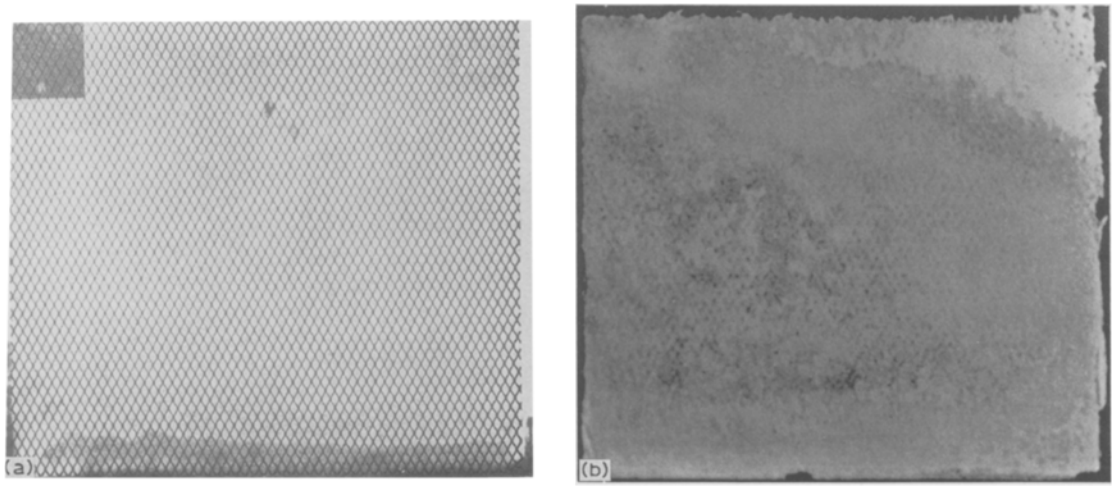

Fig. 7. Zinc electrode from Cell 25%-Ca (No. 1) after testing was terminated at cycle 151. (a) X-ray photograph, and (b) normal photograph.

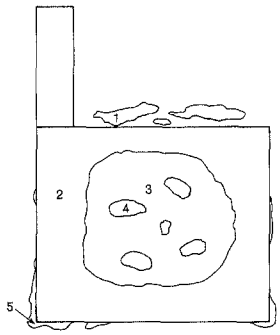

Fig. 8. Sketch showing distinct regions of a typical cycled zinc electrode. The numbers identify various types of regions. (1) Growth off the current collector at the upper edge of the electrode; (2) semi-uniform region near the edges, between island regions and the growth at the edges; (3) centre region between islands; (4) island areas; (5) dense growth off the sides (not the top) of the current collector.

zinc electrode was found to dramatically improve cycle life performance. The $Ca(OH)_2$ formed calcium zincate with the zincate-supersaturated KOH solution during the discharge half-cycle. Because calcium zincate is relatively insoluble in this solution, its formation significantly decreased the rate of zinc redistribution (shape change). These results were obtained with constant-mass negative electrodes, i.e. the amount of excess ZnO was decreased by the amount of $Ca(OH)_2$ addition, thereby maintaining high specific energy. For similarly constructed cells, the capacity utilization of the zinc material, measured as delivered Ah per unit mass of excess ZnO, increased from $\sim 20\,Ah\,g^{-1}$ for a Ca-free negative electrode to $> 75\,Ah\,g^{-1}$ for a 25 mol % $Ca(OH)_2$ electrode. Also, the 25 mol % $Ca(OH)_2$ electrode was still functioning well when cycling was terminated at 150 cycles whereas the calcium-free baseline Zn/NiOOH cell was terminated due to lack of capacity at only 64 cycles. X-ray images and chemical analyses of the discharged electrodes after cycling showed that for the calcium-containing cells, a uniform layer of 'background' calcium zincate was present whereas in the calcium-free cells there were

Table 3. Amount of ZnO found in each NiOOH electrode

Cell (No.)	*No. of Cycles*	*Amount of ZnO/g*
25%-Ca (1)	151	0.75
10%-Ca (1)	59	0.69
10%-Ca (2)	5	0.49
10%-Ca (3)	106	0.63
0%-Ca (1)	150	0.75
0%-Ca (2)	64	0.63

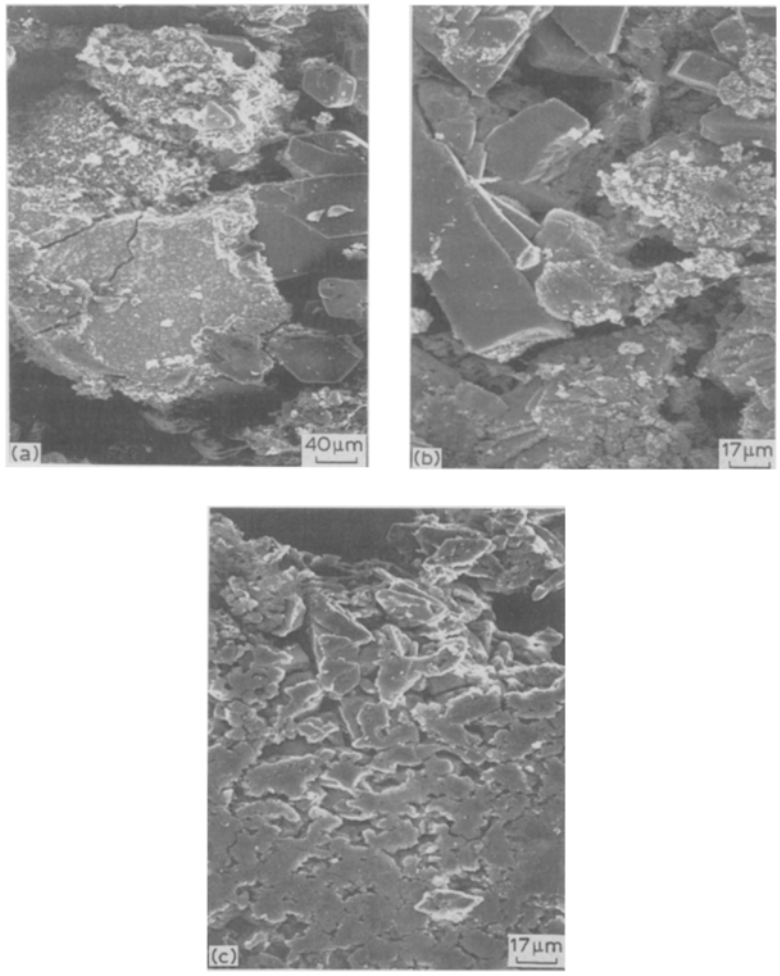

Fig. 9. Morphology of area 2 (see Fig. 8) in various zinc electrodes containing $Ca(OH)_2$. (a)–(c) Calcium zincate crystals surrounded by zinc powder.

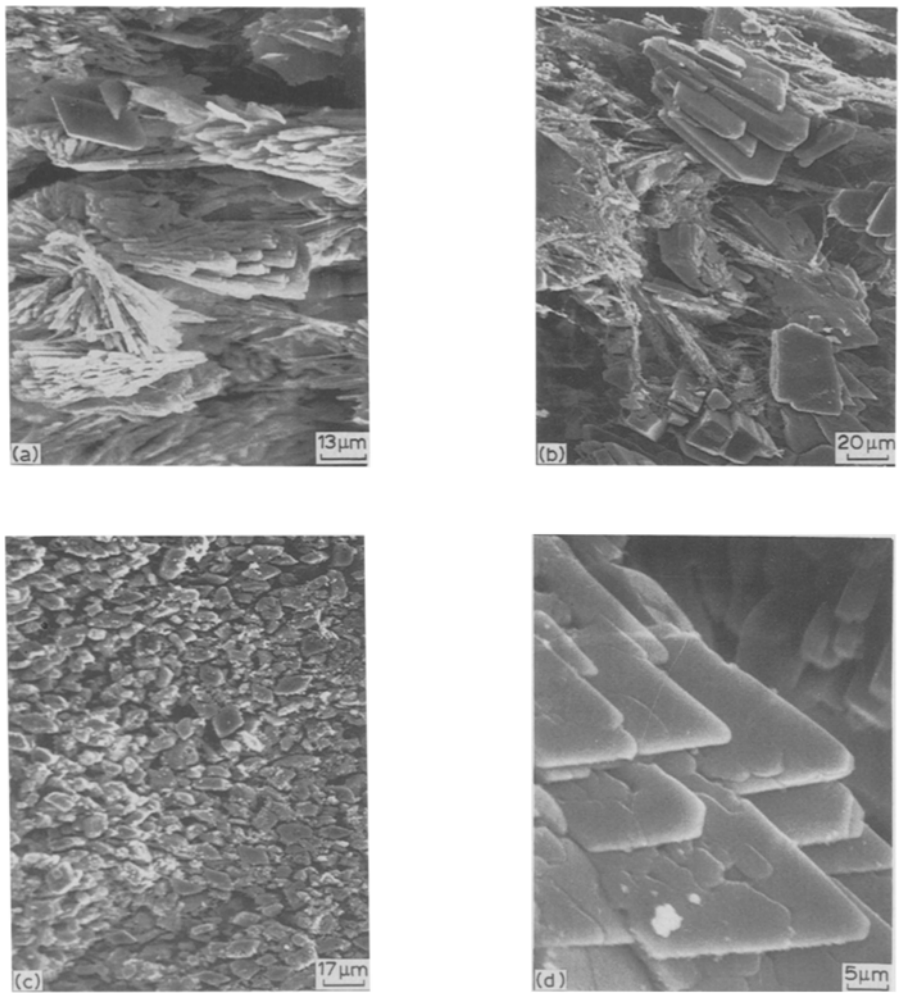

Fig. 10. Morphology of area 3 in representative zinc electrodes containing $Ca(OH)_2$. (a), (c) and (d) Calcium zincate crystals are found everywhere with very little ZnO present. Tetragonal crystals are clearly seen in (d). (b) PTFE filaments can be seen binding the crystals together.

many regions on the current collector with no Zn or ZnO.

The addition of only 10 mol % $Ca(OH)_2$ was found to be insufficient to maintain cycling capacity. While $Ca(OH)_2$ additions were found to raise the zinc electrode overpotential during charge, the increase was not sufficiently large to cause shorting or decrease the cell efficiency for the 10 and 25% $Ca(OH)_2$ cells. For the 40% $Ca(OH)_2$ cells, however, the increase in overpotential, and the expansion of the electrode itself resulted in the early failure of those cells.

A comprehensive material balance was performed on a 25% $Ca(OH)_2$ cell, and the extent of zinc migration was evaluated in all of the cells. It was found that a significant portion of the zinc migrates to the NiOOH electrodes.

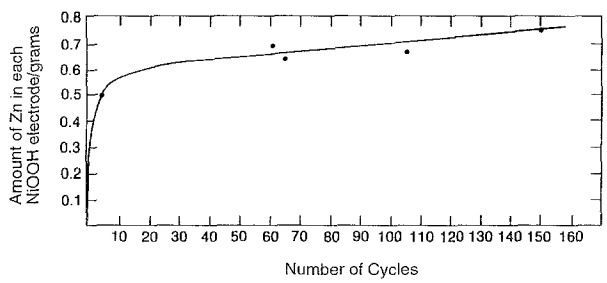

Fig. 11. Amount of zinc migration into NiOOH electrodes.

Acknowledgements

This work was supported by the Assistant Secretary for Conservation and Renewable Energy, Office of Transportation Technologies, Electric & Hybrid Propulsion Division of the U.S. Department of Energy under Contract No. DE-AC03-76SF00098.

References

[1] F. R. McLarnon and E. J. Cairns, *J. Electrochem. Soc.* **138** (1991) 645.
[2] V. V. Romanoff, *J. Appl. Chem. (USSR)* **35** (1962) 1246.
[3] N. A. Zhulidov and F. I. Efremov, *Vest. Elektroprom.* **34** (1971) 74.
[4] W. J. van der Grinten, Abstract No. 38, p. 96, The Electrochemical Society Extended Abstracts, Oct. 15–20 (1967).
[5] W. van der Grinten (General Electric Co.), *U.S. Patent 3516862* (1970).
[6] Y. Maki, M. Fujita, H. Takahashi and T. Ino (Hitachi, Ltd. and Tokyo Electric Power Co., *U.S. Patent 3816178* (1974).
[7] R. A. Jones (General Motors Corporation), *U.S. Patent 4358517* (1982).
[8] G. Kawamura and Y. Maki, *Denki Kagaku* **48** (1980) 592.
[9] W. Schwick, R. Diehl and C. D. Carpentier, *Nature (Lond.), Phys. Sci.* **229** (1971) 184.
[10] M. Yamanaka, H. Morishchi and K. Furuya (Mitsubishi Mining and Cement Co., Ltd.), *Japanese Patent 52139134* (1977).

[11] O. Ohhara and T. Fujii (Kuraray Co., Ltd.), *Japanese Patent 50 109 229* (1975).
[12] R. A. Sharma, *J. Electrochem. Soc.* **133** (1986) 2215.
[13] F. Liebau and A. Amel-Zadeh, *Kristall und Technik* **7** (1972) 221.
[14] 'International Centre for Diffraction Data Handbook' (1980) pp. 24–222.
[15] M. K. Traore, *C. R. Acad. Sc. Paris, Ser. C* **278** (1974) 1429.
[16] M. Inasaki and Y. Yamashita, *Yosyo Kyokaishi* **95** (1987) 363.
[17] E. G. Gagnon, *J. Electrochem. Soc.* **133** (1986) 1989.
[18] Y. Maki, Y. Fujita, M. Kikuchi and T. Kamimura, 'Battery Research and New Batteries in Japan', Vol. 2, paper no. 29, The Electrochemical Society of Japan (Cleveland Office), 1972.
[19] E. G. Gagnon and Y.-M. Wang, *J. Electrochem. Soc.* **134** (1987) 2091.
[20] *Idem.*, 'Prog. Batteries Sol. Cells', Vol. 7, p. 380, The Electrochemical Society of Japan (Cleveland Office), 1988.
[21] G. Kucera, H. G. Plust and C. Schneider, Paper No. 750 147 presented at the Automotive Engineering Congress and Exposition, Society of Automotive Engineers, Detroit, MI, Feb. 24–28 (1975).
[22] E. H. Hietbrink, R. W. Boak, R. L. Corbin, R. A. Jones and L. P. Atkins, Abstract No. 16, p. 26, The Electrochemical Society Extended Abstracts, Vol. 82-2, Oct. 17–21 (1982).
[23] R. A. Sharma, *J. Electrochem. Soc.* **135** (1988) 1875.
[24] Y.-M. Wang and G. Wainwright, *ibid.* **133** (1986) 1869.
[25] E. G. Gagnon, *ibid.* **138** (1991) 3173.
[26] Y.-M. Wang, *ibid.* **137** (1990) 2800.
[27] Y. Sato, M. Kanda, H. Niki, M. Ueno, K. Murata, T. Shirogami and T. Takamura, *J. Power Sources* **9** (1983) 147.
[28] T. C. Adler, F. R. McLarnon and E. J. Cairns, Proc. 22nd Intersoc. Energy Conv. Eng. Conf., p. 1097, American Institute of Aeronautics and Astronautics, New York (1987).
[29] D. M. MacArthur, proc. 20th Intersoc. Energy Convers. Eng. Conf., p. 2.27, Society of Automotive Engineers, Warrendale, PA (1985).
[30] J. McBreen, Brookhaven National Laboratory Report No. BNL-51370 (1980).
[31] R. Jain, F. R. McLarnon and E. J. Cairns, Lawrence Berkeley Laboratory Report No. LBL-25332 (1989).
[32] J. T. Nichols, F. R. McLarnon and E. J. Cairns, *Chem. Eng. Comm.* **37** (1985) 355.
[33] M. H. Katz, J. T. Nichols, F. R. McLarnon, E. J. Cairns and J. E. Katz, *J. Power Sources* **10** (1983) 149.